

# Crystalline symmetry protected number-conserving Majorana mode in Dirac semi-metal nanowires

Rui-Xing Zhang<sup>1</sup> and Chao-Xing Liu<sup>1</sup>

<sup>1</sup>Department of Physics, The Pennsylvania State University, University Park, Pennsylvania 16802

(Dated: December 14, 2024)

Majorana zero mode, a non-Abelian anyon which serves as the cornerstone for topological quantum computations, has been intensively searched in fractional quantum Hall systems and topological superconductors. Recent several works suggest that such mode can also exist in one dimensional (1D) interacting double-wire setup, and an important issue in these proposals is to suppress inter-channel single-particle tunneling that spoils the topological ground state degeneracy. Here we show that 1D Dirac semimetal (DSM) nanowire is an ideal platform to realize such number-conserving Majorana physics. By inserting magnetic flux, a DSM nanowire is driven into crystalline-symmetry-protected semimetallic phase. Interaction enables the emergence of boundary Majorana zero modes, which is robust as a result of crystalline symmetry protection. Various experimental consequences are discussed, aiming at determining Majorana modes in experiments.

*Introduction* - Anyons are natural generalizations of bosons and fermions, from the perspective of quantum statistics. Interchanging a pair of anyons can either induce a non-trivial phase factor  $e^{i\theta} \neq \pm 1$  in the wavefunction (Abelian anyons), or rotate the corresponding many-body wave function among a degenerate set of locally indistinguishable states in a unitary way (non-Abelian anyons) [1]. Anyonic physics was first studied in the context of fractional quantum Hall effect [2]. In particular, Majorana zero mode (MZM), one type of non-Abelian anyon, emerges as a quasi-particle excitation in a  $\nu = \frac{5}{2}$  Moore-Read state [3]. The non-Abelian statistics of MZM makes it a promising candidate of building a topological quantum computer [4]. Majorana physics was also studied in topological superconductor (TSC) after the pioneering works by Read and Green [5], Ivanov [6] and Kitaev [7]. In particular, Kitaev pointed out the existence of boundary MZM in a one-dimensional (1D) p-wave TSC. Such TSC is topologically distinct from a conventional superconductor due to the MZM-induced ground state degeneracy (GSD) [8]. The degenerate ground states are further labeled by  $Z_2$  fermion parity of the system, and their stability is guaranteed by this  $Z_2$  parity symmetry. This Kitaev model serves as the underlying mechanism of recent intensive experimental efforts in realizing MZM physics in 1D semiconductor devices [9, 10].

Theoretically, it is recently pointed out that MZM will become unstable in a single 1D quantum wire if strong quantum fluctuations destroy long-range superconductivity [11]. For a double-wire setup, however, MZMs can co-exist with quantum fluctuations when inter-wire single-particle hopping vanishes and pair hopping interaction dominates [11–20]. Here, pair hopping process fluctuates particle number of each quantum wire only by a multiple of 2, and an emergent  $Z_2$  parity is well defined in each wire. This emergent  $Z_2$  parity defines doubly degenerate ground states, and thus mimics the physics in Kitaev model. However, a well-known issue in the double-wire

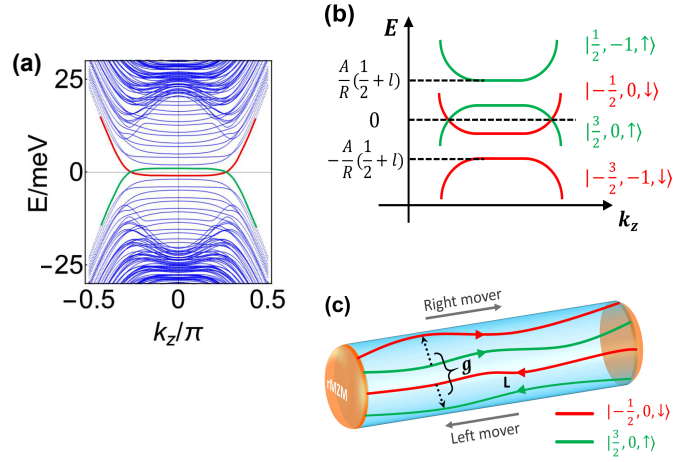


FIG. 1. As shown in (a), DSM nanowire is driven into a rotation-symmetry-protected 1D semimetal when flux  $\Phi = l\Phi_0$  ( $\frac{1}{2} < l < \frac{3}{2}$ ) is inserted. The emerging 1D Dirac points originate from  $|\frac{3}{2}, 0, \uparrow\rangle$  (green line) and  $|\frac{1}{2}, 0, \downarrow\rangle$  (red line), as shown in (b). In (c), we show the process of pair-hopping interaction  $g$ , where two “red” electrons hop to the “green” electron states simultaneously. This process respects four-fold rotation symmetry, and enables the emergence of Majorana end states.

setup comes from “ $Z_2$  parity breaking” induced by inter-wire single particle tunneling, which is generally unavoidable. Such tunneling process explicitly breaks  $Z_2$  parity of each wire and thus spoils Majorana physics.

In this work, we demonstrate that how crystalline symmetries naturally solve the “ $Z_2$  parity breaking” issue, and thus stabilize the number-conserving Majorana physics. We show that 1D nanowire of three dimensional Dirac semimetals (DSMs) [21, 22] possesses crystalline-symmetry-protected gapless Dirac points, offering us a material realization of stable semimetallic phase (Fig. 1 (a)). Therefore, a DSM nanowire manifests itself as an effective double-wire setup, with each “quantum wire” living in distinct representations of the crystalline symme-

try group. When symmetry-preserved inter-“wire” pair-hopping interaction is incorporated, the system is driven into an interaction-enabled topological phase with doubly degenerate ground states and MZMs (Fig. 1 (c)). The ground states are now labeled by distinct representations (angular momentum) of the crystalline symmetry group. Rotation symmetry naturally forbids inter-“wire” single particle tunneling and thus guarantees the stability of GSD. The boundary MZM in our setup bridges between ground states with different angular momentum representations of four-fold rotation symmetry. It is thus dubbed “representation MZM” (rMZM) to distinguish from conventional MZMs in TSCs. Experimentally, rMZM is shown to exhibit exponentially localized zero-bias peak signal, which can be detected via scanning tunneling microscopy (STM). We also propose a feasible setup to explore the transport physics of rMZM. This transport setup is identified as a novel “bined Y-junction” of three quantum wires, where the transport phase diagram and experimental signals are discussed.

*Model Hamiltonian of DSM nanowire* - The following  $k \cdot p$  Hamiltonian describes a typical DSM protected by  $C_4$  rotation symmetry[21, 22]

$$H_{k \cdot p} = \begin{pmatrix} M(k) & Ak_- & 0 & 0 \\ Ak_+ & -M(k) & 0 & 0 \\ 0 & 0 & -M(k) & -Ak_- \\ 0 & 0 & -Ak_+ & M(k) \end{pmatrix}, \quad (1)$$

The basis function  $\Psi$  is  $(|P, \frac{3}{2}\rangle, |S, \frac{1}{2}\rangle, |S, -\frac{1}{2}\rangle, |P, -\frac{3}{2}\rangle)^T$ , where spin-orbit-coupled angular momentum  $J \in \{\pm \frac{1}{2}, \pm \frac{3}{2}\}$  acts as a pseudo-spin index. Notice that  $H_{k \cdot p}$  takes a block-diagonal form of  $\text{diag}(H_\uparrow, H_\downarrow)$ , with each block describing a Weyl Hamiltonian in the corresponding spin ( $\uparrow$  or  $\downarrow$ ) sector. Here  $M(k) = M_0 - M_1 k_z^2 - M_2(k_x^2 + k_y^2)$  and  $k_\pm = k_x \pm ik_y$ , with  $A > 0$  and  $M_{0,1,2} > 0$ . The bulk Dirac points are aligned along rotational invariant  $k_z$  axis at  $k_z = \pm \sqrt{M_0/M_1}$ . The  $\uparrow$  and  $\downarrow$  sectors are related via  $H_\downarrow(M(k), A) = H_\uparrow(-M(k), -A)$ . Thus, we will focus on  $H_\uparrow$ , and the properties of  $H_\downarrow$  can be obtained analogously.

The DSM nanowire can be better described in cylindrical coordinates. We rewrite  $H_\uparrow$  in terms of  $k_r = -i\partial_r$  and  $k_\theta = -\frac{i}{r}\partial_\theta$  with angular variables  $r = \sqrt{x^2 + y^2}$  and  $\theta = \arctan \frac{y}{x}$ . Solving the eigen-state problem [23], the low-energy eigenstates of  $H_\uparrow$  are found to be Fermi arc states on the side surface of the nanowire [24]. For a nanowire with radius  $R$ , surface Fermi arc spectrum  $E_\uparrow = -\frac{A}{R}(m + \frac{1}{2})$ , where  $m = 0, \pm 1, \pm 2, \dots$  is the eigenvalue of  $k_\theta$ . The spin-down part of  $H_0$  behaves similarly with  $E_\downarrow = \frac{A}{R}(m + \frac{1}{2})$ . Notice that the complete Fermi arc spectrum always exhibits a finite gap of  $A/R$ , which originates from the  $\pi$  spin Berry phase of the Fermi arc states [25]. In this nanowire geometry, total angular momentum  $J_{tot}$  is a good quantum number, while it is actually composed of two parts: (1) angular contribution from  $k_\theta$  and (2) pseudo-spin  $J$  which is encoded in the

basis  $\Psi$ . In particular, we find that a state with  $k_\theta = m$  carries  $J_{tot} = m + 2\sigma + \frac{1}{2}$  in the spin- $\sigma$  ( $\sigma = \pm \frac{1}{2}$ ) sector. Thus, we label an energy eigen-state as  $|J_{tot}, m, \sigma\rangle$  where spin index  $\sigma \in \{\uparrow, \downarrow\}$ .

The 1D semimetallic phase can be realized by inserting magnetic flux to remove the Berry phase effect. The applied magnetic field should be precisely aligned along the nanowire to preserve the rotation symmetry of the system. With flux  $\Phi = l$  (in units of  $\Phi_0 = h/e$ ) inserted,  $E_{\uparrow/\downarrow} = \mp \frac{A}{R}(m + \frac{1}{2} - l)$ . The  $\pi$  Berry phase is exactly canceled, when  $\pi$ -flux ( $l = \frac{1}{2}$ ) is inserted. Consequently,  $|\frac{3}{2}, 0, \uparrow\rangle$  touches  $|-\frac{1}{2}, 0, \downarrow\rangle$  at  $k_z = 0$ , which is similar to the worm-hole effect of topological insulator nanowire [26]. When  $\Phi$  is further increased,  $|\frac{3}{2}, 0, \uparrow\rangle$  intersects with  $|-\frac{1}{2}, 0, \downarrow\rangle$  to form a gapless inverted band structure (1D Dirac points), as shown in Fig. 1 (b). Since  $|\frac{3}{2}, 0, \uparrow\rangle$  and  $|-\frac{1}{2}, 0, \downarrow\rangle$  belong to different representations of the rotational group, the 1D Dirac points are robust and thus protected by  $C_4$  symmetry. In Fig. 1 (a), we verify the above results in the tight-binding model obtained from regularizing the  $k \cdot p$  Hamiltonian on a cubic lattice [27]. This is how we assemble a 1D rotation-symmetry-protected semimetal by inserting magnetic flux into the DSM nanowire.

*Number-conserving Majorana physics* - To incorporate interaction effects, the low-energy theory is well captured by 2-channel Luttinger liquid (LL) theory,

$$H_0 = \sum_{s=1,2} \int dx \frac{v}{2} [\psi_{s,R}^\dagger(x) \partial_x \psi_{s,R}(x) - \psi_{s,L}^\dagger(x) \partial_x \psi_{s,L}(x)].$$

Here  $\psi_{1,R(L)}^\dagger$  creates a right (left) moving electron with  $J_{tot} = -\frac{1}{2}$ , while  $\psi_{2,R(L)}^\dagger$  creates a right (left) moving electron with  $J_{tot} = \frac{3}{2}$ . Two-particle processes that preserve both charge  $U(1)$  and  $C_4$  rotation symmetry are:

$$H_1 = \int dx [g \psi_{1,R}^\dagger \psi_{1,L}^\dagger \psi_{2,R} \psi_{2,L} + g_1 \psi_{1,R}^\dagger \psi_{2,L}^\dagger \psi_{2,R} \psi_{1,L} + g_2 \psi_{1,R}^\dagger \psi_{2,R}^\dagger \psi_{2,L} \psi_{1,L} + h.c.] \quad (2)$$

If we move the Fermi level slightly away from the Dirac points (zero energy in Fig. 1 (a) and (b)), both  $g_1$  and  $g_2$  scatterings involve certain amount of momentum transfer, and will be suppressed in a translational invariant system. Inter-channel pair-hopping  $g$ , however, preserves both momentum conservation and  $C_4$  symmetry (angular momentum transfer  $\Delta J_{tot} = 4$ ). As will be shown below, it is  $g$  that is responsible for Majorana physics.

We next apply Abelian bosonization technique and define  $\psi_{s,R} \sim e^{i\sqrt{\pi}(\phi_s - \theta_s)}$  and  $\psi_{s,L} \sim e^{-i\sqrt{\pi}(\phi_s + \theta_s)}$ . It is convenient to introduce the bonding and anti-bonding fields as  $\phi_\pm = \frac{1}{\sqrt{2}}(\phi_1 \pm \phi_2)$  and  $\theta_\pm = \frac{1}{\sqrt{2}}(\theta_1 \pm \theta_2)$ , as well as  $K_\pm$  to be the Luttinger parameters for bonding and anti-bonding channel. The bonding sector remains gapless, while the anti-bonding sector opens up a non-trivial

gap with the Hamiltonian

$$H_- = \int dx \frac{v}{2} [K_- (\partial_x \phi_-)^2 + \frac{1}{K_-} (\partial_x \theta_-)] + g \int dx \cos 2\sqrt{2\pi} \theta_-. \quad (3)$$

We will focus on  $K_- < 1$  where  $g$  is relevant under renormalization group analysis. At Luther-Emery point ( $K_- = \frac{1}{2}$ ), Eq. 3 can be exactly mapped to the topological Kitaev model with MZM end states [12]. Such mapping is achieved by repermionizing Eq. 3 with  $\tilde{\psi}_R \sim e^{i\sqrt{\pi}(\tilde{\phi}-\tilde{\theta})}$  and  $\tilde{\psi}_L \sim e^{-i\sqrt{\pi}(\tilde{\phi}+\tilde{\theta})}$ , where  $\tilde{\phi} = \phi_-/\sqrt{2}$  and  $\tilde{\theta} = \sqrt{2}\theta_-$ . Away from  $K_- = \frac{1}{2}$ , the above mapping fails while we will show that Majorana physics (both GSD and Majorana end states) persists.

The ground state is obtained by minimizing  $\cos 2\sqrt{2\pi} \theta_-$  and pinning  $\theta_- = (n_\theta + \frac{1}{2})\sqrt{\pi/2}$ , where  $n_\theta \in \mathbb{Z}$  is an integer-valued operator. Since  $\theta_-$  has  $\sqrt{2\pi}$  periodicity, there are two degenerate ground states  $|\theta_- = \pm \frac{1}{2}\sqrt{\frac{\pi}{2}}\rangle$ . To characterize the ground states, we define a “representation parity” operator  $P_r$  which counts the parity of electron number in  $J_{tot} = -\frac{1}{2}$  subspace,

$$P_r = (-1)^{\sqrt{\frac{1}{\pi}} \int_0^L dx \partial_x \phi_1} = P_+ P_-, \quad (4)$$

where a nanowire with finite length  $L$  is considered and  $P_\pm = e^{i\sqrt{\pi/2}(\phi_\pm(L) - \phi_\pm(0))}$ . With  $P_r \theta_- P_r^{-1} = \theta_- - \sqrt{\frac{\pi}{2}}$ ,  $P_r$  interchanges  $|\theta_- = \pm \frac{1}{2}\sqrt{\frac{\pi}{2}}\rangle$  from one to another. Quantum superposition principle, however, allows us to define the following degenerate ground states,

$$|\pm\rangle = \frac{1}{\sqrt{2}} [|\theta_- = \frac{1}{2}\sqrt{\frac{\pi}{2}}\rangle \pm |\theta_- = -\frac{1}{2}\sqrt{\frac{\pi}{2}}\rangle], \quad (5)$$

where  $|+\rangle$  and  $|-\rangle$  are characterized by even and odd  $P_r$  parity, respectively. Since  $P_r$  is a global property of the system, the degeneracy here is topological, which can NOT be distinguished via any local measurement.

Topological GSD can also be revealed by constructing rMZM operators explicitly. Imposing open boundary condition at  $x = 0$  gives rise to  $\psi_{l,L}(0) + \psi_{l,R}(0) = 0$  for  $l = 1, 2$ , which corresponds to  $\phi_l(0) = n_l^{(1)}\sqrt{\pi}$  up to an unimportant constant. Here,  $n_l^{(1)} \in \mathbb{Z}$  is an integer-valued operator. Introducing  $n_+^{(1)} = n_1^{(1)} + n_2^{(1)}$  and  $n_-^{(1)} = n_1^{(1)}$ , the boundary condition fixes the value of  $\phi_\pm$  as  $\phi_+(0) = n_+^{(1)}\sqrt{\pi/2}$  and  $\phi_-(0) = (2n_-^{(1)} - n_+^{(1)})\sqrt{\pi/2}$ . It is important to notice that  $[n_-^{(1)}(x), n_\theta(x')] = \frac{i}{\pi}\Theta(x - x')$ , while  $n_+^{(1)}$  always commutes with  $n_\theta$  and behaves like a c-number. Following Ref. [28], we construct rMZM operator  $\alpha_1$  at  $x = 0$  and  $\alpha_2$  at  $x = L$  as,

$$\alpha_1 = e^{i\pi(n_-^{(1)} + n_\theta)}, \quad (6)$$

$$\alpha_2 = e^{i\pi(n_-^{(2)} + n_\theta)}, \quad (7)$$

where we have defined the boundary condition at  $x = L$  to be  $\phi_+(L) = n_+^{(2)}\sqrt{\pi/2}$  and  $\phi_-(L) = (2n_-^{(2)} - n_+^{(2)})\sqrt{\pi/2}$  in a similar way. The Majorana properties of  $\alpha_{1,2}$  can be easily checked, where  $[\alpha_{1,2}, H_-] = 0$  and  $\alpha_1^2 = \alpha_2^2 = 1$ . Starting from a ground state  $|+\rangle$ , one can easily show that  $\alpha_{1,2}|+\rangle = |-\rangle$  up to some phase factors. This also proves the topological GSD.

It should be noted that  $C_4$  symmetry is playing an essential role in protecting Majorana physics. In particular, inter-channel single particle tunneling event is strictly prohibited to preserve  $C_4$  symmetry, which in return stabilizes the GSD. Besides,  $C_4$  symmetry breaks down to a  $Z_2$  symmetry in the low energy subspace and is equivalent to representation parity  $P_r$  in the ground state manifold, with  $C_4|\pm\rangle = \pm|\pm\rangle$ . Therefore, rMZM  $\alpha_{1,2}$  can be interpreted as a “bridge” connecting different representations of the crystalline symmetry group.

*Experimental detection* - In 1D TSCs, MZM is a superposition of an electron state and a hole state. Thus, it serves as a resonant level for an external electron to hop onto, which leads to resonant Andreev reflection effect [29]. In interacting DSM nanowires, however, the absence of long-range superconductivity puts a question mark on the possibility of a similar effect. It is less clear that whether and how these rMZMs will behave under the existing experimental approaches.

To address this question, we consider a tunneling problem from a Fermi liquid lead to the DSM nanowire. This tunneling process changes both electron number and representation parity  $P_r$  simultaneously. In particular, the ground state is changed from  $|0\rangle = |N, p\rangle$  with  $N$  electrons and  $P_r = p$  to  $|1\rangle = |N+1, -p\rangle$  with  $N+1$  electrons and  $P_r = -p$  via this tunneling process. We compute the spatial feature of spectral density that is directly related to STM experimentally. For a DSM nanowire at  $x \in [0, L]$ , in the  $L \rightarrow \infty$  limit, transition matrix element of injecting a single electron at  $x = x_0$  ( $0 \leq x_0 \ll L$ ) can be calculated with the help of mode expansion technique [23, 30], and the resulting spectral density is

$$\rho(x, \omega \rightarrow 0) = |\langle 1|\psi_{1,R}^\dagger|0\rangle|^2 + |\langle 1|\psi_{1,R}|0\rangle|^2 = \mathcal{N}(x, \epsilon, K_\pm) e^{-\frac{\pi}{4K_\pm} \frac{x}{\xi}} \quad (8)$$

where  $\xi = \sqrt{\frac{v}{8\pi g K_-}}$  is the correlation length of the system and  $\epsilon$  is the short distance cut-off. While  $\mathcal{N}(x, \epsilon, K_\pm)$  counts the power-law contribution of this transition process [23], the exponential part of  $\rho(x, \omega \rightarrow 0)$  ambiguously reveals an exponentially localized rMZM on the boundary, which is ready to be detected using STM technique. Since  $\xi \sim 1/\sqrt{g}$ , the stronger the interaction, the more localized rMZM will be.

Finally, we will generalize the above setup to a transport problem with a Luttinger liquid lead (similar ideas have been widely discussed in TSC/LL junction [31]). Our proposed transport setup can be feasibly realized

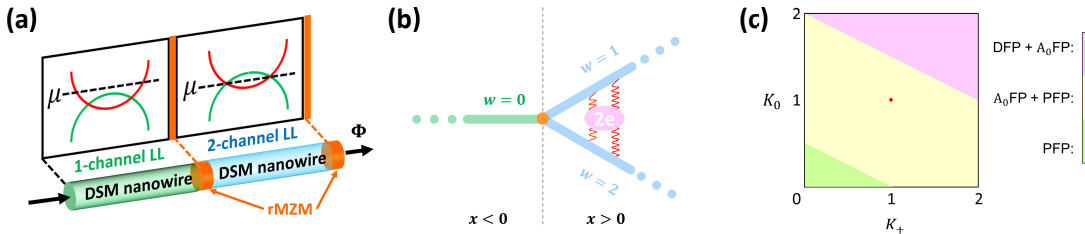


FIG. 2. (a) We apply a step-function gate to DSM nanowire, where the 1-channel LL acts as a LL lead. (b) A systematic plot of banded Y-junction. (c) Transport phase diagram of banded Y-junction, where the red dot denotes the non-interacting limit.

in experiment by applying a step-function-like gating to the DSM nanowire, as shown in Fig. 2 (a). Gaplessness of bonding sector, however, distinguishes our setup from conventional TSC/LL junction by introducing additional degree of freedom in the low-energy theory. In particular, three inequivalent Luttinger parameters ( $K_0$ ,  $K_+$  and  $K_-$ ) show up in the low-energy theory, where  $K_0$  is the Luttinger parameter of LL lead. This greatly enhances the complexity of boundary conditions at  $x = 0$ . From a different perspective, our setup can be viewed as a “Y”-shaped junction of three quantum “wires” with wire index  $w = 0, 1, 2$ . As shown in Fig. 2 (b), two quantum wires ( $w = 1, 2$ ) are banded via inter-wire interaction  $g$ , which is thus dubbed “*binded Y-junction*”. Up to our knowledge, this kind of setup has never been explored in existing literatures.

To attack this complex transport problem, the recently developed “delayed evaluation of boundary condition” (DEBC) method [32, 33] is adopted to identify renormalization group fixed points (FPs) and evaluate scaling dimensions of perturbation terms at each FP. A brief introduction of this method and details of FP information can be found in the supplementary materials [23]. The phase diagram of banded Y-junction is mapped out in Fig. 2 (c) for  $K_- < 1$ . In the strongly attractive regime ( $K_+ < 1 - 2K_0$ ), pair-tunneling fixed point (PFP) is stable, where electrons tend to pair up and tunnel among three wires, and greatly enhances tunneling conductance. This mimics the Andreev reflection effect in a TSC/LL junction, and PFP is also called “Andreev reflection FP” in earlier literatures [32]. In the strongly repulsive limit ( $K_+ > 4 - 2K_0$ ), two stable FPs are found to co-exist: (i) “Disconnecting FP” (DFP), where wire  $w = 0, 1, 2$  are disconnected from each other and inter-wire tunneling is quenched. (ii) “Asymmetric  $A_0$  FP” ( $A_0$ FP) [34], where  $w = 1$  and  $w = 2$  are connected via pair tunneling, while tunnelings from  $w = 0$  to  $w = 1, 2$  are quenched.

A realistic system is most likely to fall into the weakly interacting regime ( $K_0, K_+ \approx 1$ ), as plotted in yellow in Fig. 2 (c). Here, there exists both stable PFP and  $A_0$ FP. In transport measurement, one expects a zero-bias conductance peak at PFP, while vanishing conductance at  $A_0$ FP. The co-existence of two stable FPs suggests the emergence of an intermediate unstable FP which charac-

terizes the transition between PFP and  $A_0$ FP. This novel phase transition is quite intriguing, which is definitely worthy to be explored in future works. At last, the role of rMZM is explored by mapping out a Majorana-free phase diagram where we quench pair-hopping interaction  $g$  at  $x > 0$ . In this case, we find a completely different phase diagram with more exotic phases [23]. Specially, the system falls into  $A_0$ FP near  $K_{0,+} \approx 1$ , while PFP only shows up in the strongly attractive regime. Therefore, the appearance of weakly interacting PFP in Fig. 2 (c) is a direct consequence of rMZM, and serves as a transport evidence of Majorana physics.

*Discussion* - In summary, we have proposed that magnetic-flux insertion drives DSM nanowire into a 1D crystalline-symmetry-protected semimetal, which serves as an ideal platform to realize number-conserving Majorana physics. In particular, crystalline symmetry forbids inter-channel single-particle tunneling, and thus guarantees the stability of Majorana physics. We notice that DSM nanowire of  $\text{Cd}_3\text{As}_2$  has been successfully fabricated [35, 36], while these nanowires have been grown along [112] direction, so that  $C_4$  rotation symmetry is explicitly broken. Experimentally, we expect that correlated DSM material with [001] growth direction will be very promising candidates to realize number-conserving Majorana physics. In our discussion, we create only one pair of Dirac points with flux number  $\frac{1}{2} < l < \frac{3}{2}$ . In general, one can keep increasing flux to create more 1D Dirac points, realizing a  $N$ -channel LL ( $N > 2$ ) system [23]. Such  $N$ -channel LL could be a potential realization of coupled wire system, whose interaction effects have been widely discussed [37–40]. In addition, the Majorana mechanism we proposed can be easily generalized to 1D metals/semimetals protected by other crystalline symmetries (such as mirror symmetry, three-fold and six-fold rotation symmetry etc.) or internal symmetries, which is definitely a promising direction to be explored.

*Acknowledgement* - The authors are indebted to Meng Cheng for valuable suggestions. R.-X.Z would like to thank Jian-Xiao Zhang, Jiabin Yu and Jiahua Gu for helpful discussions, and particularly Lun-Hui Hu for collaboration on a closely related project. C.-X. L. and R.-X.Z acknowledge support from Office of Naval Research (Grant No. N00014-15-1-2675).

---

[1] C. Nayak, S. H. Simon, A. Stern, M. Freedman, and S. D. Sarma, *Reviews of Modern Physics* **80**, 1083 (2008).

[2] D. C. Tsui, H. L. Stormer, and A. C. Gossard, *Physical Review Letters* **48**, 1559 (1982).

[3] G. Moore and N. Read, *Nuclear Physics B* **360**, 362 (1991).

[4] A. Y. Kitaev, *Annals of Physics* **303**, 2 (2003).

[5] N. Read and D. Green, *Physical Review B* **61**, 10267 (2000).

[6] D. A. Ivanov, *Physical Review Letters* **86**, 268 (2001).

[7] A. Y. Kitaev, *Physics-Uspekhi* **44**, 131 (2001).

[8] J. Alicea, *Reports on Progress in Physics* **75**, 076501 (2012).

[9] R. M. Lutchyn, J. D. Sau, and S. D. Sarma, *Physical review letters* **105**, 077001 (2010).

[10] Y. Oreg, G. Refael, and F. von Oppen, *Physical review letters* **105**, 177002 (2010).

[11] L. Fidkowski, R. M. Lutchyn, C. Nayak, and M. P. Fisher, *Physical Review B* **84**, 195436 (2011).

[12] M. Cheng and H.-H. Tu, *Physical Review B* **84**, 094503 (2011).

[13] J. D. Sau, B. Halperin, K. Flensberg, and S. D. Sarma, *Physical Review B* **84**, 144509 (2011).

[14] C. V. Kraus, M. Dalmonte, M. A. Baranov, A. M. Läuchli, and P. Zoller, *Physical review letters* **111**, 173004 (2013).

[15] G. Ortiz, J. Dukelsky, E. Cobanera, C. Esebbag, and C. Beenakker, *Physical review letters* **113**, 267002 (2014).

[16] J. Klinovaja and D. Loss, *Physical review letters* **112**, 246403 (2014).

[17] F. Iemini, L. Mazza, D. Rossini, R. Fazio, and S. Diehl, *Physical review letters* **115**, 156402 (2015).

[18] N. Lang and H. P. Büchler, *Physical Review B* **92**, 041118 (2015).

[19] C. Chen, W. Yan, C. Ting, Y. Chen, and F. Burnell, *arXiv preprint arXiv:1701.01794* (2017).

[20] F. Iemini, L. Mazza, L. Fallani, P. Zoller, R. Fazio, and M. Dalmonte, *Physical Review Letters* **118**, 200404 (2017).

[21] Z. Wang, Y. Sun, X.-Q. Chen, C. Franchini, G. Xu, H. Weng, X. Dai, and Z. Fang, *Physical Review B* **85**, 195320 (2012).

[22] Z. Wang, H. Weng, Q. Wu, X. Dai, and Z. Fang, *Physical Review B* **88**, 125427 (2013).

[23] See Supplementary Materials for details.

[24] K.-I. Imura and Y. Takane, *Physical Review B* **84**, 245415 (2011).

[25] In the limit  $R \rightarrow \infty$ , the energy gap in both spin sectors approaches zero and DSM nanowire evolves into a bulk DSM sample with two bulk Dirac points connected by Fermi arc states.

[26] G. Rosenberg, H.-M. Guo, and M. Franz, *Physical Review B* **82**, 041104 (2010).

[27] The nanowire configuration is modeled by taking periodic (open) boundary condition along the  $z$  ( $x$  and  $y$ ) direction. Realistic parameters of  $\text{Cd}_2\text{As}_3$  are applied in the calculation, and the cross section in the  $x$ - $y$  plane is chosen to be a  $16 \times 16$  square.

[28] D. J. Clarke, J. Alicea, and K. Shtengel, *Nature Communications* **4**, 1348 (2013).

[29] K. T. Law, P. A. Lee, and T. K. Ng, *Physical review letters* **103**, 237001 (2009).

[30] A. Keselman and E. Berg, *Physical Review B* **91**, 235309 (2015).

[31] L. Fidkowski, J. Alicea, N. H. Lindner, R. M. Lutchyn, and M. P. Fisher, *Physical Review B* **85**, 245121 (2012).

[32] M. Oshikawa, C. Chamon, and I. Affleck, *Journal of Statistical Mechanics: Theory and Experiment* **2006**, P02008 (2006).

[33] C.-Y. Hou, A. Rahmani, A. E. Feiguin, and C. Chamon, *Physical Review B* **86**, 075451 (2012).

[34] The subscript 0 comes from the fact that wire  $w = 0$  is disconnected from the other two wires.

[35] C.-Z. Li, L.-X. Wang, H. Liu, J. Wang, Z.-M. Liao, and D.-P. Yu, *Nature communications* **6** (2015).

[36] L.-X. Wang, C.-Z. Li, D.-P. Yu, and Z.-M. Liao, *Nature communications* **7** (2016).

[37] C. Kane, R. Mukhopadhyay, and T. Lubensky, *Physical review letters* **88**, 036401 (2002).

[38] J. C. Teo and C. Kane, *Physical Review B* **89**, 085101 (2014).

[39] T. Neupert, C. Chamon, C. Mudry, and R. Thomale, *Physical Review B* **90**, 205101 (2014).

[40] E. Sagi and Y. Oreg, *Physical Review B* **90**, 201102 (2014).

## Supplementary Materials for “Crystalline symmetry protected number-conserving Majorana mode in Dirac semi-metal nanowires”

### APPENDIX A. DIRAC SEMIMETAL IN CYLINDRICAL COORDINATES

In this appendix, we will follow Ref. [24] to derive the low-energy theory of DSM nanowire in a cylindrical geometry. A typical Hamiltonian for Dirac semimetals (such as  $\text{Na}_3\text{Bi}$  and  $\text{Cd}_3\text{As}_2$ ) is given by [21, 22]

$$H_{\text{Dirac}} = \begin{pmatrix} H_{\uparrow} & 0 \\ 0 & H_{\downarrow} \end{pmatrix} = \begin{pmatrix} M(k) & Ak_- & 0 & 0 \\ Ak_+ & -M(k) & 0 & 0 \\ 0 & 0 & -M(k) & -Ak_- \\ 0 & 0 & -Ak_+ & M(k) \end{pmatrix}. \quad (9)$$

The basis functions are  $|P, \frac{3}{2}\rangle, |S, \frac{1}{2}\rangle, |S, -\frac{1}{2}\rangle, |P, -\frac{3}{2}\rangle$ . Here  $M(k) = M_0 - M_1 k_z^2 - M_2 (k_x^2 + k_y^2)$  and  $k_{\pm} = k_x \pm ik_y$ , with  $A > 0$  and  $M_{0,1,2} > 0$ . The bulk Dirac points are  $k_z = \pm K_0 = \pm \sqrt{\frac{M_0}{M_1}}$ . Notice that  $H_{\downarrow}(M(k), A) = H_{\uparrow}(-M(k), -A)$  and we will focus on  $H_{\uparrow}$  in the following discussion. In cylindrical coordinate,  $(x, y, z) \rightarrow (r, \theta, z)$  with

$$r = \sqrt{x^2 + y^2}, \quad \theta = \arctan \frac{y}{x}. \quad (10)$$

It is easy to show that

$$\begin{aligned} k_+ &= e^{i\theta}(k_r + ik_{\theta}) \\ k_- &= e^{-i\theta}(k_r - ik_{\theta}) \end{aligned} \quad (11)$$

with  $k_r = -i\frac{\partial}{\partial r}$  and  $k_{\theta} = -i\frac{1}{r}\frac{\partial}{\partial \theta}$ . When the radius  $r$  is much larger than the lattice constant  $a$  with  $r \gg a$ , we also have  $k_x^2 + k_y^2 = k_r^2 + k_{\theta}^2$ . Then  $H_{\uparrow}$  can be separated into  $H_{\uparrow, \perp}$  describing the physics normal to the surface and  $H_{\uparrow, \parallel}$  describing the physics parallel to the surface. Let us consider the physics around some  $k_0$  on the  $k_z$  axis, with  $k_z = k_0 + \delta k_z$ . For simplicity, we will use  $k_z$  to represent  $\delta k_z$  in the later discussion. We find that

$$H_{\uparrow, \perp} = \begin{pmatrix} N(k_0) - M_2 k_r^2 & Ae^{-i\theta} k_r \\ Ae^{i\theta} k_r & -N(k_0) + M_2 k_r^2 \end{pmatrix} \quad (12)$$

and

$$H_{\uparrow, \parallel} = \begin{pmatrix} -2M_1 k_0 k_z - M_1 k_z^2 - M_2 k_{\theta}^2 & -iAe^{-i\theta} k_{\theta} \\ iAe^{i\theta} k_{\theta} & 2M_1 k_0 k_z + M_1 k_z^2 + M_2 k_{\theta}^2 \end{pmatrix}. \quad (13)$$

Here  $N(k_0) = M_0 - M_1 k_0^2$ . The strategy here is to solve for eigenstate of  $H_{\uparrow, \perp}$  with open boundary condition and use this result to project  $H_{\uparrow, \parallel}$  to extract low-energy effective theory of the Dirac semimetal nanowire. Let us assume the radius of the nanowire is  $R \gg a$ , and the open boundary condition is  $\psi_{\perp}(r = R) = 0$ . Then a trial wavefunction of  $H_{\uparrow, \perp}$  should take the form

$$\psi_{\perp, \lambda}(r) \sim e^{\lambda(r-R)} \begin{pmatrix} C \\ De^{i\theta} \end{pmatrix} \quad (14)$$

Then the energy eigenstate with energy  $E$  can be shown to take the form

$$\psi_{\perp, \lambda}(E, r) \sim e^{\lambda(r-R)} \begin{pmatrix} E + m(\lambda) \\ -i\lambda Ae^{i\theta} \end{pmatrix} \quad (15)$$

where  $m(\lambda) = N_0 + M_2 \lambda^2$ . On the other hand, eigen-equation now becomes

$$\det \begin{pmatrix} m(\lambda) - E & -iAe^{-i\theta} \lambda \\ -iAe^{i\theta} \lambda & -m(\lambda) - E \end{pmatrix} = 0 \quad (16)$$

$\lambda_{\pm}$  are the two positive  $\lambda$  solutions of the above equation, and they satisfy

$$\lambda_{+} \lambda_{-} = \sqrt{\frac{N_0^2 - E^2}{M_2^2}} \quad (17)$$

Notice that these solutions only exist when  $|E| < |N_0|$ . This implies that the surface state solutions are in-gap states which live at  $-k_0 < k_z < k_0$ . The wavefunction now can be written as a linear superposition of  $\lambda_+$  and  $\lambda_-$  eigenstates,

$$\psi_{\perp}(E, r) = c_+ e^{\lambda_+(r-R)} \psi_{\perp, \lambda_+} + c_- e^{\lambda_-(r-R)} \psi_{\perp, \lambda_-} \quad (18)$$

The boundary condition at  $r = R$  indicates that

$$\det \begin{pmatrix} m(\lambda_+) + E & m(\lambda_-) + E \\ -iAe^{i\theta} \lambda_+ & -iAe^{i\theta} \lambda_- \end{pmatrix} = 0 \quad (19)$$

After some calculations, we find that

$$E(E + N_0) = 0 \quad (20)$$

For  $|E| < |N_0|$ , the only solution is

$$\begin{aligned} E &= 0 \\ m(\lambda) &= \pm A\lambda \end{aligned} \quad (21)$$

Together with the definition of  $m(\lambda)$ ,  $\lambda_{\pm}$  must satisfy

$$M_2 \lambda^2 \mp A\lambda + N_0 = 0 \quad (22)$$

or equivalently

$$\begin{aligned} \lambda_+ + \lambda_- &= \pm \frac{A}{2M_2} \\ \lambda_+ \lambda_- &= \frac{N_0}{M_2} \end{aligned} \quad (23)$$

Since  $\lambda_{\pm} > 0$ , we have  $m(\lambda) = A\lambda$  and  $N_0 > 0$ , which implies  $|k_0| < \frac{M_0}{M_1} = K_0$ . Therefore, this in-gap surface states only exists between two bulk Dirac points, and are identified as the Fermi arc states connecting the bulk Dirac points. The surface state wavefunction now takes the form

$$\psi_{\perp}(E, r, \theta) = f(\lambda_{\pm}, r) \begin{pmatrix} 1 \\ -ie^{i\theta} \end{pmatrix} \quad (24)$$

Now let us obtain the projected low energy theory of  $H_{\uparrow, \parallel}$ , and we find that

$$\begin{aligned} H_{\uparrow, \text{eff}} &= \psi_{\perp}^{\dagger} H_{\uparrow, \parallel} \psi_{\perp} \\ &= -\frac{A}{r} \left( -i \frac{\partial}{\partial \theta} + \frac{1}{2} \right) + \frac{M_2}{r^2} \left( 1 - 2i \frac{\partial}{\partial \theta} \right) \end{aligned} \quad (25)$$

With periodic boundary condition along  $\hat{\theta}$  direction,  $k_{\theta}$  is a good quantum number and  $-i\partial_{\theta}$  operator takes integer values  $m = 0, 1, 2, 3, \dots$ . It is easy to see that the lowest energy state locates at  $r = R$ , and when  $R \gg a$ , the second term in  $H_{\uparrow, \text{eff}}$  can be ignored. We find that

$$E_{\uparrow, \text{eff}} = -\frac{A}{R} \left( m + \frac{1}{2} \right). \quad (26)$$

As for the spin-down part, since  $H_{\downarrow}(M(k), A) = H_{\uparrow}(-M(k), -A)$ , it is easy to see that

$$E_{\downarrow, \text{eff}} = \frac{A}{R} \left( m + \frac{1}{2} \right). \quad (27)$$

It is easy to see that the energy spectrum is gapped because of the  $\pi$  Berry phase which gives rise to a  $\frac{A}{R}$  energy gap.

To remove the Berry phase effect, we apply a magnetic field, which must be carefully aligned along the nanowire to preserve the rotation symmetry of the system. Assume the flux is  $\Psi = l\Psi_0$  with  $\Psi_0 = \frac{\hbar}{e}$  being the flux quantum, the energy spectrum is modified to

$$\begin{aligned} E_{\uparrow, \text{eff}} &= -\frac{A}{R} \left( m + \frac{1}{2} - l \right) \\ E_{\downarrow, \text{eff}} &= \frac{A}{R} \left( m + \frac{1}{2} - l \right) \end{aligned} \quad (28)$$

Therefore, inserting magnetic flux shifts  $E_{\uparrow,eff}$  by  $\frac{lA}{R}$  and  $E_{\downarrow,eff}$  by  $-\frac{lA}{R}$ . When  $l > \frac{1}{2}$ , we find that  $|m = 0, \uparrow\rangle$  ( $m = 0$  state in the spin up sector) and  $|m = 0, \downarrow\rangle$  form gapless inverted band structure, leading to semimetallic dispersions.

As a result of Eq. 24, a state labeled with  $m$  can be written as

$$\begin{aligned} |m, \uparrow\rangle &\sim e^{im\theta} |\psi_{\perp}, \uparrow\rangle = e^{im\theta} \left( \left| \frac{3}{2} \right\rangle - ie^{i\theta} \left| \frac{1}{2} \right\rangle \right) \\ |m, \downarrow\rangle &\sim e^{im\theta} |\psi_{\perp}, \downarrow\rangle = e^{im\theta} \left( \left| -\frac{1}{2} \right\rangle - ie^{i\theta} \left| -\frac{3}{2} \right\rangle \right) \end{aligned} \quad (29)$$

where we have ignored its  $r$  and  $k_z$  dependence. Therefore, even with the same  $m$  value, the spin-up state and the spin-down state have different angular momentum. Their angular momentum can be read out when we apply a rotation operator  $C_{\theta} = e^{iJ\theta}$ , and we find that

$$\begin{aligned} C_{\theta} |m, \uparrow\rangle &= e^{i(m+\frac{3}{2})\theta} |m, \uparrow\rangle \quad \text{with } J = m + \frac{3}{2} \\ C_{\theta} |m, \downarrow\rangle &= e^{i(m-\frac{1}{2})\theta} |m, \downarrow\rangle \quad \text{with } J = m - \frac{1}{2} \end{aligned} \quad (30)$$

Therefore,  $|m = 0, \uparrow\rangle$  carries angular momentum  $J = \frac{3}{2}$  while  $|m = 0, \downarrow\rangle$  carries angular momentum  $J = -\frac{1}{2}$ . These two states belong to different representations of rotation group, and the crossing between them is protected.

## APPENDIX B. EQUIVALENCE BETWEEN $C_4$ SYMMETRY AND $Z_2$ PARITY SYMMETRY

According to the angular momentum representation,  $C_4$  acts on the dual bosonic fields as,

$$C_4 \begin{pmatrix} \phi_+ \\ \phi_- \\ \theta_+ \\ \theta_- \end{pmatrix} = \begin{pmatrix} \phi_+ \\ \phi_- \\ \theta_+ - \frac{1}{2}\sqrt{\frac{\pi}{2}} \\ \theta_- + \sqrt{\frac{\pi}{2}} \end{pmatrix} \quad (31)$$

Thus,  $C_4$  symmetry also interchanges  $|\theta_- = \pm\frac{1}{2}\sqrt{\frac{\pi}{2}}\rangle$ , which indicates that the degenerate ground states  $|\pm\rangle$  are also eigen-states of  $C_4$  symmetry operator. This proves the equivalence between  $C_4$  symmetry and  $Z_2$  parity in the low-energy sector.

## APPENDIX C. DIAGONALIZING $H_-$ WITH MODE EXPANSION

In this appendix, we introduce mode expansion technique to explicitly diagonalize the anti-bonding Hamiltonian  $H_-$ . The mode expansion offers us a powerful weapon to attack the electron tunneling problem. We introduce,

$$\begin{aligned} \phi_-(x) &= \sqrt{\frac{\pi}{2}}(n_{\phi} + \frac{1}{2}) + \sqrt{\frac{\pi}{2}} \frac{\Delta n x}{L} + \frac{1}{\sqrt{\pi}} \sum_{k=1}^{\infty} \sqrt{\frac{1}{K_- k}} \sin \frac{\pi k x}{L} (a_k + a_k^{\dagger}) \\ \theta_-(x) &= \sqrt{\frac{\pi}{2}}(n_{\theta} + \frac{1}{2}) + \sqrt{\frac{\pi}{2}} \theta_0 - i \frac{1}{\sqrt{\pi}} \sum_{k=1}^{\infty} \sqrt{\frac{K_-}{k}} \cos \frac{\pi k x}{L} (a_k - a_k^{\dagger}) \end{aligned} \quad (32)$$

with  $[\Delta n, \theta_0] = i$  and  $[a_k, a_{k'}^{\dagger}] = \delta_{k,k'}$ . Here, we have expanded the cosine term in  $H_-$  around its minimum as  $4\pi g[\theta_- - (n_{\theta} + \frac{1}{2})\sqrt{\frac{\pi}{2}}]^2$ . Plug in the mode expansion (Eq. 32) to the Hamiltonian and after some tedious calculations, we obtain that

$$\begin{aligned} \frac{v}{2} K_- \int dx (\partial_x \phi_-)^2 &= \frac{v\pi}{4L} (\Delta n)^2 + \sum_k \frac{v\pi k}{4L} [a_k a_k^{\dagger} + a_k^{\dagger} a_k + (a_k)^2 + (a_k^{\dagger})^2] \\ \frac{v}{2} \frac{1}{K_-} \int dx (\partial_x \theta_-)^2 &= - \sum_k \frac{v\pi k}{4L} [-a_k a_k^{\dagger} - a_k^{\dagger} a_k + (a_k)^2 + (a_k^{\dagger})^2] \\ 4\pi g[\theta_- - (n_{\theta} + \frac{1}{2})\sqrt{\frac{\pi}{2}}]^2 &= 2gL\pi^2 \theta_0^2 - \sum_k \frac{2gLK_-}{k} [-a_k a_k^{\dagger} - a_k^{\dagger} a_k + (a_k)^2 + (a_k^{\dagger})^2] \end{aligned} \quad (33)$$

Therefore,

$$H_- = \frac{v\pi}{4L}(\Delta n)^2 + 2gL\pi^2\theta_0^2 + \sum_k \frac{A_k}{2}[a_k a_k^\dagger + a_k^\dagger a_k] - \sum_k \frac{B_k}{2}[(a_k)^2 + (a_k^\dagger)^2]. \quad (34)$$

With

$$\begin{aligned} A_k &= \frac{v\pi k}{L} + \frac{4gLK_-}{k} \\ B_k &= \frac{4gLK_-}{k} \end{aligned} \quad (35)$$

Introduce the following Bogoliubov transformations

$$\begin{aligned} \Delta n &= \left(\frac{8g\pi L^2}{v}\right)^{\frac{1}{4}} \frac{d + d^\dagger}{\sqrt{2}} \\ \theta_0 &= \left(\frac{8g\pi L^2}{v}\right)^{-\frac{1}{4}} \frac{d - d^\dagger}{i\sqrt{2}} \\ a_k &= C_k \alpha_k + D_k \alpha_k^\dagger \end{aligned} \quad (36)$$

where  $C_k = \sqrt{\frac{1}{2}(\frac{A_k}{E_k} + 1)}$  and  $D_k = \sqrt{\frac{1}{2}(\frac{A_k}{E_k} - 1)}$ . The Bogoliubov quasi-particles satisfy commutation relations as  $[d, d^\dagger] = 1$  and  $[\alpha_k, \alpha_{k'}^\dagger] = \delta_{k,k'}$ . The energy function  $E_k$  is now given by  $E_k = \sqrt{A_k^2 - B_k^2}$ , and it is closely related to the energy dispersion of the system

$$H_- = \sqrt{\frac{vg\pi^3}{2}} d^\dagger d + \sum_k E_k \alpha_k^\dagger \alpha_k \quad (37)$$

Let us have a closer look at the form of  $E_k$ . By defining  $q = \frac{\pi k}{L}$ , we find a very nice form

$$E_k = \sqrt{v^2 q^2 + \Delta^2} \quad (38)$$

where  $\Delta = \sqrt{8\pi v g K_-}$  physically denotes the energy gap formed in the anti-bonding sector, which originates from pair-hopping interaction  $g$ .

#### APPENDIX D. TRANSITION AMPLITUDE OF ELECTRON TUNNELING PROBLEM

When an electron of  $s = 1$  tunnels into the system, it changes the sign of both total Fermi parity  $P_{tot}$  and representation parity  $P$ . Therefore, the original ground state  $|0\rangle = |N, p\rangle$  is changed to  $|1\rangle = |N + 1, -p\rangle$  via this tunneling process, with  $p \in \pm 1$ . On the other hand, the total charge  $Q_+$  and the charge in channel  $s = 1$  are given by

$$\begin{aligned} Q_+ &= \sqrt{\frac{2}{\pi}} [\phi_+(L) - \phi_+(0)], \\ Q_1 &= \sqrt{\frac{1}{\pi}} [\phi_1(L) - \phi_1(0)] = \frac{1}{2}(Q_+ + Q_-) \end{aligned} \quad (39)$$

Since  $\Delta Q_+ = \Delta Q_1 = 1$  during this single electron tunneling, we find that  $\Delta Q_+ = \Delta Q_- = 1$ , or equivalently

$$\Delta\phi_+ = \Delta\phi_- = \sqrt{\frac{\pi}{2}}. \quad (40)$$

where we have defined  $\Delta\phi_\pm = \phi_\pm(L) - \phi_\pm(0)$ . Here it is convenient to parameterize  $\Delta\phi_\pm(x) = \sqrt{\frac{\pi}{2}}(1 - \frac{x}{L})$ . The two ground states can be connected via a unitary transformation  $|1\rangle = e^{-i\eta}|0\rangle$  [30], where  $\eta = \eta_+ + \eta_-$  and

$$\begin{aligned} \eta_+ &= \int dx \Delta\phi_+ \partial_x \theta_+ \\ \eta_- &= \int dx \Delta\phi_- \partial_x \theta_- \end{aligned} \quad (41)$$

With the fact that  $[e^{-i\eta_{\pm}}, \phi_{\pm}(x)] = \Delta\phi_{\pm}(x)e^{-i\eta_{\pm}}$ , it is easy to show that  $e^{-i\eta_{\pm}}\phi_{\pm}(x)e^{i\eta_{\pm}} = \phi_{\pm}(x) + \Delta\phi_{\pm}(x)$ .

Next, we would like to calculate the tunneling amplitude

$$\begin{aligned}\langle 1|\psi_{1,R}^{\dagger}|0\rangle &= \langle 0|e^{i\eta}e^{-i\sqrt{\pi}(\phi_1-\theta_1)}|0\rangle \\ &= \langle e^{i\eta_+}e^{-i\sqrt{\frac{\pi}{2}}(\phi_+-\theta_+)}\rangle_+ \times \langle e^{i\eta_-}e^{-i\sqrt{\frac{\pi}{2}}(\phi_--\theta_-)}\rangle_- \\ &= T_+T_-\end{aligned}\quad (42)$$

Let us first focus on the anti-bonding part,

$$\begin{aligned}T_- &= \langle e^{i\eta_-}e^{-i\sqrt{\frac{\pi}{2}}(\phi_--\theta_-)}\rangle_- \\ &= e^{-\frac{1}{2}\langle[\eta_- - \sqrt{\frac{\pi}{2}}(\phi_--\theta_-)]^2\rangle_-}\end{aligned}\quad (43)$$

### Contribution from $T_-$

With the mode expansion in Eq. 32, let us move on to calculate  $T_-$ . For  $\delta_-$

$$\begin{aligned}\eta_- &= \int dx \Delta\phi_- \partial_x \theta_- \\ &= \frac{i}{\sqrt{2}} \sum_k \sqrt{\frac{K}{k}} \frac{\pi k}{L} (a_k - a_k^{\dagger}) \int_0^L dx (1 - \frac{x}{L}) \sin \frac{\pi kx}{L} \\ &= i \sqrt{\frac{K}{2}} \sum_k \frac{a_k - a_k^{\dagger}}{\sqrt{k}}\end{aligned}\quad (44)$$

Notice that in  $T_- = e^{-F_-}$ , the imaginary part in  $F_- = \frac{1}{2}\langle[\eta_- - \sqrt{\frac{\pi}{2}}(\phi_--\theta_-)]^2\rangle_-$  only contributes to a phase factor, while its amplitude originates from its real part. By ignoring the imaginary part, we find that

$$F_- = \frac{1}{2}\langle[\eta_- + \sqrt{\frac{\pi}{2}}\theta_-]^2\rangle_- + \frac{\pi}{4}\langle\phi_-^2\rangle_- \quad (45)$$

To start with

$$\eta_- + \sqrt{\frac{\pi}{2}}\theta_- = i \sum_k \sqrt{\frac{K_-}{2k}} (a_k - a_k^{\dagger}) (1 - \cos \frac{\pi kx}{L}) + \frac{\pi}{2}(n_{\theta} + \theta_0 + \frac{1}{2}) \quad (46)$$

In the following discussion, we will ignore the  $\theta_0$  and  $\Delta n$  part, which will give rise to a universal contribution to  $T_-$  as

$$e^{-\frac{\pi^2}{8}[(n_{\theta}+\frac{1}{2})^2 + (n_{\phi}+\frac{1}{2})^2]} \times e^{-\frac{\pi^2}{16L}(\sqrt{\frac{v}{8g\pi}} + \sqrt{\frac{8g\pi}{v}}x^2)} \quad (47)$$

where the second term becomes unity as  $L \rightarrow \infty$ . Then

$$\begin{aligned}\langle[\eta_- + \sqrt{\frac{\pi}{2}}\theta_-]^2\rangle_- &= - \sum_{k,k'} \frac{K_-}{2} \frac{1}{\sqrt{kk'}} (1 - \cos \frac{\pi kx}{L}) (1 - \cos \frac{\pi k'x}{L}) (a_k - a_k^{\dagger})(a_{k'} - a_{k'}^{\dagger}) \\ &= \sum_k (C_k - D_k)^2 \frac{K_-}{2k} (1 - \cos \frac{\pi kx}{L})^2\end{aligned}\quad (48)$$

where we have used  $\langle\alpha_k^{\dagger}\alpha_k\rangle = 0$ . Let us define  $\kappa = \xi^{-1} = \frac{\Delta}{v}$ ,

$$\begin{aligned}A_k &= vq + \frac{\Delta^2}{2qv} = v(q + \frac{\kappa^2}{2q}) \\ B_k &= v \frac{\kappa^2}{2q}\end{aligned}\quad (49)$$

In the strong coupling limit  $\Delta \rightarrow \infty$ ,  $\kappa \gg q$ . Then  $A_k \approx B_k \approx v \frac{\kappa^2}{2q}$  and  $E_k \approx v\kappa$ . We find that

$$(C_k - D_k)^2 \approx \frac{q}{\kappa} \quad (50)$$

By taking  $L \rightarrow \infty$ ,

$$\begin{aligned} \frac{1}{2} \langle [\eta_- + \sqrt{\frac{\pi}{2}} \theta_-]^2 \rangle_- &= \frac{K_-}{4\kappa} \int dq (1 - \cos qx)^2 \times e^{-\epsilon q} \\ &= \frac{3K_- \xi}{8} \end{aligned} \quad (51)$$

where we have introduced a decay factor  $e^{-\epsilon q}$  as the short distance divergence, and  $\epsilon$  is the short distance cut-off. Therefore, this part of  $F_-$  does not have spatial dependence. For the second part of  $F_-$ ,

$$\begin{aligned} \frac{\pi}{4} \langle \phi_-^2 \rangle_- &= \frac{1}{4K_-} \sum_{k,k'} \sqrt{\frac{1}{kk'}} \sin \frac{\pi kx}{L} \sin \frac{\pi k'x}{L} (a_k + a_k^\dagger)(a_{k'} + a_{k'}^\dagger) \times e^{-\epsilon q} \\ &= \frac{1}{4K_-} \sum_k \frac{(C_k + D_k)^2}{k} \sin^2 \frac{\pi kx}{L} \times e^{-\epsilon q} \\ &= \frac{\kappa}{4K_-} \int dq \frac{\sin^2 qx}{q^2} \times e^{-\epsilon q} \\ &= \frac{\kappa}{4K_-} [x \arctan \frac{2x}{\epsilon} - \frac{1}{4} \epsilon \log(\frac{4x^2 + \epsilon^2}{\epsilon^2})] \\ &= \frac{\pi}{8K_-} \frac{x}{\xi} - \frac{\epsilon}{8K_- \xi} \log \frac{2x}{\epsilon} \end{aligned} \quad (52)$$

Finally, we arrive at the following important result,

$$T_- \sim \left(\frac{2x}{\epsilon}\right)^{\frac{\epsilon}{8K_- \xi}} \times e^{-\frac{\pi}{8K_- \xi} \frac{x}{\epsilon}} \quad (53)$$

### Contribution from $T_+$

Since the bonding part is gapless, we expect it only gives a power-law correction to  $T$ . To see this, we notice that the essential difference between bonding and anti-bonding physics lies in the existence of  $g$ . By setting  $g = 0$  in anti-bonding sector, one should be able to recover the physics in the bonding sector. In this limit, we find that

$$\Delta = 0, E_k = A_k = vq, B_k = 0. \quad (54)$$

This gives rise to  $C_k = 1$  and  $D_k = 0$ . Then

$$\begin{aligned} \frac{1}{2} \langle [\eta_+ + \sqrt{\frac{\pi}{2}} \theta_+]^2 \rangle_+ &= \frac{K_+}{4} \int dq \frac{(1 - \cos qx)^2}{q} \times e^{-\epsilon q} \\ &= \frac{K_+}{4} [\log \frac{x^2 + \epsilon^2}{\epsilon^2} - \frac{1}{4} \log \frac{4x^2 + \epsilon^2}{\epsilon^2}] \end{aligned} \quad (55)$$

and

$$\begin{aligned} \frac{\pi}{4} \langle \phi_+^2 \rangle_+ &= \frac{1}{4K_+} \int dq \frac{\sin^2 qx}{q} \times e^{-\epsilon q} \\ &= \frac{1}{16K_+} \log \frac{4x^2 + \epsilon^2}{\epsilon^2} \end{aligned} \quad (56)$$

Then we arrive at

$$T_+ = \left(\frac{\epsilon^2}{x^2 + \epsilon^2}\right)^{\frac{K_+}{4}} \left(\frac{4x^2 + \epsilon^2}{\epsilon^2}\right)^{\frac{1}{16}(K_+ - \frac{1}{K_+})} \quad (57)$$

Together with the anti-bonding contribution, we conclude that the single electron tunneling amplitude is given by

$$\langle 1 | \psi_{1,R}^\dagger | 0 \rangle = \mathcal{N}(x, \epsilon, K_\pm) e^{-\frac{\pi}{8K_- \xi} \frac{x}{\epsilon}}. \quad (58)$$

where  $\mathcal{N}(x, \epsilon, K_\pm)$  denotes the power-law corrections.

## APPENDIX E. GENERAL FORMALISM OF DEBC METHOD

In this appendix, we briefly review the general formalism of “delayed evaluation of boundary condition” (DEBC) method [32], and how this method can help us to evaluate scaling dimension of operators with given boundary conditions. To start with, let us consider  $N$  quantum wires with different Luttinger parameter  $K_i$  ( $i = 1, 2, \dots, N$ ) meet at  $x = 0$  and form a junction. The bosonized Hamiltonian is given by

$$H = \sum_{i=1}^N \int dx [K_i (\partial_x \phi_i)^2 + \frac{1}{K_i} (\partial_x \theta_i)^2] \quad (59)$$

where abelian bosonization is defined as

$$\begin{aligned} \psi_{i,R} &\sim e^{i\sqrt{\pi}\chi_{i,R}} = e^{i\sqrt{\pi}(\phi_i - \theta_i)} \\ \psi_{i,L} &\sim e^{-i\sqrt{\pi}\chi_{i,L}} = e^{-i\sqrt{\pi}(\phi_i + \theta_i)} \end{aligned} \quad (60)$$

It is convenient to rescale the dual fields to make the system effectively non-interacting,

$$\begin{aligned} \tilde{\phi}_i &= \sqrt{K_i} \phi_i, \quad \tilde{\theta}_i = \frac{1}{\sqrt{K_i}} \theta_i \\ \tilde{\chi}_{i,R} &= \tilde{\phi}_i - \tilde{\theta}_i, \quad \tilde{\chi}_{i,L} = \tilde{\phi}_i + \tilde{\theta}_i \end{aligned} \quad (61)$$

The boundary condition is demonstrated by

$$\vec{\chi}_R = \mathcal{O} \vec{\chi}_L \quad (62)$$

where  $\vec{\chi}_{R/L} = (\tilde{\chi}_{1,R/L}, \tilde{\chi}_{2,R/L}, \dots, \tilde{\chi}_{N,R/L})^T$ .  $\mathcal{O}$  is an orthogonal matrix with  $\mathcal{O}\mathcal{O}^T = 1$ , which contains key information of boundary condition. In other words, **a particular choice of  $\mathcal{O}$  determines certain type of conformal invariant boundary condition, which corresponds to certain RG fixed point in the tunneling phase diagram.**

To be specific, perturbations of a boundary fixed point come from tunneling or backscattering process, which generally can be written as

$$g_{m,n} \sim e^{i\sqrt{\pi}(\mathbf{m} \cdot \vec{\phi} + \mathbf{n} \cdot \vec{\theta})} \quad (63)$$

where  $\vec{\phi} = (\tilde{\phi}_1, \tilde{\phi}_2, \dots, \tilde{\phi}_N)^T$  and  $\vec{\theta} = (\tilde{\theta}_1, \tilde{\theta}_2, \dots, \tilde{\theta}_N)^T$ . With the definition of  $\mathcal{O}$  matrix, the boundary condition can be easily implemented in the  $\tilde{\chi}_{R,L}$  basis. Thus,

$$\begin{aligned} g_{m,n} &\sim e^{i\frac{\sqrt{\pi}}{2}[(\mathbf{m}+\mathbf{n}) \cdot \vec{\chi}_R + (\mathbf{m}-\mathbf{n}) \cdot \vec{\chi}_L]} \\ &= e^{i\frac{\sqrt{\pi}}{2}[\mathcal{O}^T(\mathbf{m}+\mathbf{n}) + (\mathbf{m}-\mathbf{n})]^T \vec{\chi}_L} \end{aligned} \quad (64)$$

Its scaling dimension is

$$\Delta[g_{m,n}] = \frac{1}{8} |\mathcal{O}^T(\mathbf{m} + \mathbf{n}) + (\mathbf{m} - \mathbf{n})|^2 \quad (65)$$

The specific form of  $\mathcal{O}$  depends on the boundary condition we impose.

### Orthogonality of $\mathcal{O}$ matrix

The orthogonality condition turns out to be an important and strong constraint to  $\mathcal{O}$ , which can be proved as follows. Consider an operator  $g_{A,B} = e^{i\frac{\sqrt{\pi}}{2}(\mathbf{A} \cdot \vec{\chi}_R + \mathbf{B} \cdot \vec{\chi}_L)}$ , with  $\mathbf{A}$  and  $\mathbf{B}$  both  $N$ -component vectors. From Eq. 62,  $\vec{\chi}_L = \mathcal{O}^{-1} \vec{\chi}_R$ . Then

$$\begin{aligned} g_{A,B} &= e^{i\frac{\sqrt{\pi}}{2}(\mathbf{A}^T \mathcal{O} + \mathbf{B}^T) \vec{\chi}_L} \\ &= e^{i\frac{\sqrt{\pi}}{2}(\mathbf{A}^T + \mathbf{B}^T \mathcal{O}^{-1}) \vec{\chi}_R} \end{aligned} \quad (66)$$

In terms of  $\vec{\chi}_L$ , the scaling dimension of  $g_{A,B}$  is

$$\begin{aligned}\Delta(g_{A,B}) &= \frac{1}{8}|\mathbf{A}^T \mathcal{O} + \mathbf{B}^T|^2 \\ &= \frac{1}{8}[\mathcal{O}^T(\mathbf{A}\mathbf{A}^T)\mathcal{O} + \mathbf{B}\mathbf{B}^T + \mathcal{O}^T\mathbf{A}\mathbf{B}^T + \mathbf{B}\mathbf{A}^T\mathcal{O}] \\ &= \frac{1}{8}[|\mathbf{A}|^2\mathcal{O}^T\mathcal{O} + |\mathbf{B}|^2 + (\mathcal{O}^T + \mathcal{O})\mathbf{A} \cdot \mathbf{B}]\end{aligned}\quad (67)$$

In terms of  $\vec{\chi}_R$ , we find that

$$\begin{aligned}\Delta(g_{A,B}) &= \frac{1}{8}|\mathbf{A}^T + \mathbf{B}^T\mathcal{O}^{-1}|^2 \\ &= \frac{1}{8}[|\mathbf{A}|^2 + (\mathcal{O}\mathcal{O}^T)^{-1}|\mathbf{B}|^2 + (\mathcal{O} + \mathcal{O}^T)^{-1})\mathbf{A} \cdot \mathbf{B}].\end{aligned}\quad (68)$$

To make Eq. 67 and Eq. 68 self-consistent, orthogonality condition  $\mathcal{O}\mathcal{O}^T = 1$  must be satisfied.

### Application of DEBC to binded Y-junction

Now, we are ready to apply the DEBC method to our binded Y-junction setup. The central task here is to identify  $\mathcal{O}$  matrix that characterizes physical RG fixed point. Across the junction, current conservation requires

$$J_{x<0} + J_{x>0} = 0 \quad (69)$$

Here  $J_{x<0} = -\sqrt{\frac{1}{\pi}}\partial_t\phi_0$  and  $J_{x>0} = -\sqrt{\frac{1}{\pi}}\partial_t(\phi_1 + \phi_2) = \sqrt{\frac{2}{\pi}}\partial_t\phi_+$ . The rescaling rule of fields can be defined similar to Eq. 61, with  $i = 0, \pm$ . Then the current conservation condition becomes

$$\partial_t\left(\frac{1}{\sqrt{K_0}}\phi_0 + \sqrt{\frac{2}{K_+}}\phi_+\right) = 0 \quad (70)$$

Other information of  $\mathcal{O}$  depends on the details of boundary conditions. Once we obtain  $\mathcal{O}$ , it is important to write down possible tunneling or backscattering operators that could perturb the fixed point.

(i) *Single electron tunneling*,

$$T_{ij}^s = \psi_{i,R}^\dagger \psi_{j,L} + h.c. \sim \cos \sqrt{\pi}[(\phi_i + \phi_j) - (\theta_i - \theta_j)], \quad (71)$$

where  $i \neq j \in \{0, 1, 2\}$ . However, electron tunneling process should conserve angular momentum, and only  $T_{01}^s$  and  $T_{10}^s$  are allowed. For future purpose, let us define  $T_+^s = T_{10}^s$  and  $T_-^s = T_{01}^s$ .

(ii) *Single electron backscattering*,

$$B_i = \psi_{i,L}^\dagger \psi_{i,R} + h.c. \sim \cos 2\sqrt{\pi}\phi_i, \quad (72)$$

with  $i \in \{0, 1, 2\}$ .

(iii) *Pair electron tunneling*,

$$T_{ij}^p = \psi_{i,R}^\dagger \psi_{i,L}^\dagger \psi_{j,R} \psi_{j,L} + h.c. \sim \cos 2\sqrt{\pi}(\theta_i - \theta_j) \quad (73)$$

with  $i < j \in \{0, 1, 2\}$ .

### APPENDIX F. PHASE DIAGRAM OF MAJORANA-FREE Y-JUNCTION

In this section, let us first ignore pair hopping interaction between  $i = 1$  and  $i = 2$  that pins  $\theta_-$ . Then the system is very similar to a conventional “Y” junction composed of three independent quantum wires, while rMZM does NOT show up at the junction. Yet an essential difference from previous work [32, 33] comes from the constraint of angular momentum conservation. For our purpose, we will focus on the situation where  $K_- < 1$ .

To identify a fixed point, an effective way is to assume that some electron operators have vanishing scaling dimensions. This ansatz immediately leads to a corresponding  $\mathcal{O}$  matrix. With this  $\mathcal{O}$  matrix, we first check its orthogonality condition to verify its validity. A stable fixed point is confirmed when all possible perturbations are found to be irrelevant, with the help of Eq. 65. Below, we first use “disconnecting fixed point” as a detailed example to demonstrate how DEBC method extract the information of a fixed point. Then we will exhaust physical RG fixed points and discuss their stability problem.

### Disconnecting fixed point: an tutorial of DEBC method

The disconnecting fixed point is characterized by the vanishing scaling dimension of all the backscattering processes  $B_{0,1,2}$ . Thanks to the current conservation, the vanishing scaling dimension of two backscattering operators will automatically leads to zero scaling dimension of the remaining backscattering operator. Physically, this simply means that if wire  $w = 0$  and  $w = 1$  are both disconnected,  $w = 2$  is also forced to be disconnected at the junction as no electron can flow from  $w = 0, 1$  to  $w = 2$ .

We first define  $\vec{\chi}_{R/L} = (\tilde{\chi}_{0,R/L}, \tilde{\chi}_{+,R/L}, \tilde{\chi}_{-,R/L})^T$ , following the convention in Eq. 61. The backscattering operators are now:

$$\begin{aligned} B_0 &\sim \cos \sqrt{\pi} \left( \frac{\tilde{\chi}_{0,R} + \tilde{\chi}_{0,L}}{\sqrt{K_0}} \right) \\ B_1 &\sim \cos \sqrt{\pi} \left[ \frac{\tilde{\chi}_{+,R} + \tilde{\chi}_{+,L}}{\sqrt{2K_+}} + \frac{\tilde{\chi}_{-,R} + \tilde{\chi}_{-,L}}{\sqrt{2K_-}} \right] \\ B_2 &\sim \cos \sqrt{\pi} \left[ \frac{\tilde{\chi}_{+,R} + \tilde{\chi}_{+,L}}{\sqrt{2K_+}} - \frac{\tilde{\chi}_{-,R} + \tilde{\chi}_{-,L}}{\sqrt{2K_-}} \right] \end{aligned} \quad (74)$$

Let us re-examine Eq. 64 and Eq. 65, the only way to make  $\Delta[g_{m,n}] = 0$  is to impose

$$(\mathbf{m} + \mathbf{n}) \cdot \vec{\chi}_R + (\mathbf{m} - \mathbf{n}) \cdot \vec{\chi}_L = 0. \quad (75)$$

Therefore, we impose Eq. 75 to  $B_0$  and  $B_1$ . Together with the current conservation condition, we arrive at

$$\begin{aligned} \frac{\tilde{\chi}_{0,R} + \tilde{\chi}_{0,L}}{\sqrt{K_0}} &= 0 \\ \frac{\tilde{\chi}_{+,R} + \tilde{\chi}_{+,L}}{\sqrt{2K_+}} + \frac{\tilde{\chi}_{-,R} + \tilde{\chi}_{-,L}}{\sqrt{2K_-}} &= 0 \\ \frac{\tilde{\chi}_{0,R} + \tilde{\chi}_{0,L}}{2\sqrt{K_0}} + \frac{\tilde{\chi}_{+,R} + \tilde{\chi}_{+,L}}{\sqrt{2K_+}} &= 0 \end{aligned} \quad (76)$$

It is quite easy to see the solution of the above equations as

$$\tilde{\chi}_{w,R} = -\tilde{\chi}_{w,L}, \quad \forall w \in \{0, 1, 2\}, \quad (77)$$

which immediately leads to the rotation matrix  $\mathcal{O}_D$  that characterizes disconnecting fixed point according to its definition (Eq. 62):

$$\mathcal{O}_D = \begin{pmatrix} -1 & 0 & 0 \\ 0 & -1 & 0 \\ 0 & 0 & -1 \end{pmatrix}. \quad (78)$$

Physically, Eq. 77 implies

$$\phi_0 = \phi_+ = \phi_- = 0. \quad (79)$$

which is recognized as the disconnecting boundary condition at the junction. The scaling dimensions of electron

operators can be calculated via Eq. 65,

$$\begin{aligned}
\Delta(T_+^s) &= \frac{1}{4}(2K_0 + K_+ + K_-) \\
\Delta(T_-^s) &= \frac{1}{4}(2K_0 + K_+ + K_-) \\
\Delta(T_{01}^p) &= 2K_0 + K_+ + K_- \\
\Delta(T_{12}^p) &= 4K_- \\
\Delta(T_{20}^p) &= 2K_0 + K_+ + K_- \\
\Delta(B_0) &= 0 \\
\Delta(B_1) &= 0 \\
\Delta(B_2) &= 0.
\end{aligned} \tag{80}$$

When all tunneling terms are irrelevant, we require

$$\begin{aligned}
K_0 &> \frac{(4 - K_-) - K_+}{2} \\
K_- &> \frac{1}{4}
\end{aligned} \tag{81}$$

This condition explicitly characterizes the region in the tunneling phase diagram where DFP is stable.

### Pair-tunneling fixed point

At the pair-tunneling fixed point, two-electron pair-tunneling process  $T_{ij}^P$  is dominating, and

$$\mathcal{O}_P = \begin{pmatrix} -1 + \frac{4K_0}{2K_0 + K_+} & -\frac{2\sqrt{2K_0 K_+}}{2K_0 + K_+} & 0 \\ -\frac{2\sqrt{2K_0 K_+}}{2K_0 + K_+} & 1 - \frac{4K_0}{2K_0 + K_+} & 0 \\ 0 & 0 & 1 \end{pmatrix}. \tag{82}$$

The  $\mathcal{O}_P$  matrix is obtained similarly to  $\mathcal{O}_D$  matrix in Eq. 78 in the last section. From  $\mathcal{O}_P$ , it is easy to tell that

$$\phi_0 = -\sqrt{2}\phi_+, \quad \theta_+ = \sqrt{2}\theta_0, \quad \theta_- = 0. \tag{83}$$

The scaling dimensions at this fixed point are

$$\begin{aligned}
\Delta(T_+^s) &= \frac{1}{4}\left(\frac{1}{2K_0 + K_+} + \frac{1}{K_-}\right) \\
\Delta(T_-^s) &= \frac{1}{4}\left(\frac{1}{2K_0 + K_+} + \frac{1}{K_-}\right) \\
\Delta(T_{01}^p) &= 0 \\
\Delta(T_{12}^p) &= 0 \\
\Delta(T_{20}^p) &= 0 \\
\Delta(B_0) &= \frac{4}{2K_0 + K_+} \\
\Delta(B_1) &= \frac{1}{2K_0 + K_+} + \frac{1}{K_-} \\
\Delta(B_2) &= \frac{1}{2K_0 + K_+} + \frac{1}{K_-}.
\end{aligned} \tag{84}$$

Pair-tunneling fixed point is stable when

$$\begin{aligned}
\frac{1}{2K_0 + K_+} + \frac{1}{K_-} &> 4 \\
2K_0 + K_+ &< 4
\end{aligned} \tag{85}$$

Thus

$$K_0 < \frac{C_p - K_+}{2} \quad (86)$$

where  $C_p = 4$  if  $K_- \leq \frac{1}{4}$  and  $C_p = \min\{4, (4 - \frac{1}{K_-})^{-1}\}$  if  $K_- > \frac{1}{4}$ .

$\chi_+$  fixed point

$\chi_+$  fixed point is defined so that  $T_+^s$  is the only term whose scaling dimension is vanishing, and thus dominates the junction physics. We find that

$$\mathcal{O}_+ = \frac{1}{1 + K_-(2K_0 + K_+)} \begin{pmatrix} -1 + K_-(2K_0 - K_+) & -2K_- \sqrt{2K_0 K_+} & 2\sqrt{2K_0 K_-} \\ -2K_- \sqrt{2K_0 K_+} & -1 - K_-(2K_0 - K_+) & -2\sqrt{K_+ K_-} \\ -2\sqrt{2K_0 K_-} & 2\sqrt{K_+ K_-} & -1 + K_-(2K_0 + K_+) \end{pmatrix}. \quad (87)$$

From  $\mathcal{O}_+$ , this simply means

$$\phi_0 = -\sqrt{2}\phi_+ = \sqrt{2}\theta_-, \quad \phi_- = \theta_+ - \sqrt{2}\theta_0. \quad (88)$$

The scaling dimensions at this fixed point are

$$\begin{aligned} \Delta(T_+^s) &= 0 \\ \Delta(T_-^s) &= \frac{2K_0 + K_+ + K_-}{1 + K_-(2K_0 + K_+)} \\ \Delta(T_{01}^p) &= \frac{2K_0 + K_+ + K_-}{1 + K_-(2K_0 + K_+)} \\ \Delta(T_{12}^p) &= \frac{4K_-}{1 + K_-(2K_0 + K_+)} \\ \Delta(T_{20}^p) &= \frac{2K_0 + K_+ + K_-}{1 + K_-(2K_0 + K_+)} \\ \Delta(B_0) &= \frac{4K_-}{1 + K_-(2K_0 + K_+)} \\ \Delta(B_1) &= \frac{2K_0 + K_+ + K_-}{1 + K_-(2K_0 + K_+)} \\ \Delta(B_2) &= \frac{2K_0 + K_+ + K_-}{1 + K_-(2K_0 + K_+)}. \end{aligned} \quad (89)$$

$\chi_+$  fixed point is stable when

$$\begin{aligned} [1 - (2K_0 + K_+)](1 - K_-) &< 0 \\ K_- [4 - (2K_0 + K_+)] &> 1 \end{aligned} \quad (90)$$

Since  $K_- < 1$ , we find that

$$\begin{aligned} \frac{1 - K_+}{2} &< K_0 < \frac{(4 - \frac{1}{K_-}) - K_+}{2} \\ \text{and } K_- &> \frac{1}{3} \end{aligned} \quad (91)$$

$\chi_-$  fixed point

When  $T_-^s$  is dominating, we arrive at the  $\chi_-$  fixed point, with

$$\mathcal{O}_- = \frac{1}{1 + K_-(2K_0 + K_+)} \begin{pmatrix} -1 + K_-(2K_0 - K_+) & -2K_- \sqrt{2K_0 K_+} & -2\sqrt{2K_0 K_-} \\ -2K_- \sqrt{2K_0 K_+} & -1 - K_-(2K_0 - K_+) & 2\sqrt{K_+ K_-} \\ 2\sqrt{2K_0 K_-} & -2\sqrt{K_+ K_-} & -1 + K_-(2K_0 + K_+) \end{pmatrix}. \quad (92)$$

and

$$\phi_0 = -\sqrt{2}\phi_+ = -\sqrt{2}\theta_-, \quad \phi_- = -\theta_+ + \sqrt{2}\theta_0. \quad (93)$$

Notice the difference and similarity between  $\mathcal{O}_+$  and  $\mathcal{O}_-$ . It is easy to check that  $\chi_-$  fixed point shares the same scaling dimensions of  $T_{ij}^p$  and  $B_i$  with those of  $\chi_+$  fixed point. The only change in scaling dimension is that

$$\begin{aligned} \Delta(T_+^s) &= \frac{2K_0 + K_+ + K_-}{1 + K_-(2K_0 + K_+)} \\ \Delta(T_-^s) &= 0 \end{aligned} \quad (94)$$

Therefore, when Eq. 90 is satisfied, both  $\chi_+$  and  $\chi_-$  fixed points are stable. In other words,  $\chi_+$  and  $\chi_-$  fixed points coexist, and we expect an interesting intermediate unstable fixed point which characterizes the phase transition between these two fixed points.

### $A_0$ fixed point

Asymmetric fixed point  $A_i$  takes place when wire  $i$  is disconnected to the rest of the junction, while the other two wires are fully connected via electron tunneling process. For  $A_0$  fixed point,  $B_0$  and  $T_{12}^p$  will have vanishing scaling dimension, with

$$\mathcal{O}_{A_0} = \begin{pmatrix} -1 & 0 & 0 \\ 0 & -1 & 0 \\ 0 & 0 & 1 \end{pmatrix}. \quad (95)$$

and

$$\phi_0 = \phi_+ = \theta_- = 0. \quad (96)$$

The scaling dimensions at this fixed point are

$$\begin{aligned} \Delta(T_+^s) &= \frac{1 + K_-(2K_0 + K_+)}{4K_-} \\ \Delta(T_-^s) &= \frac{1 + K_-(2K_0 + K_+)}{4K_-} \\ \Delta(T_{01}^p) &= 2K_0 + K_+ \\ \Delta(T_{12}^p) &= 0 \\ \Delta(T_{20}^p) &= 2K_0 + K_+ \\ \Delta(B_0) &= 0 \\ \Delta(B_1) &= \frac{1}{K_-} \\ \Delta(B_2) &= \frac{1}{K_-}. \end{aligned} \quad (97)$$

For  $K_- < 1$ ,  $B_{1,2}$  are always irrelevant under RG. Thus,  $A_0$  fixed point is stable when

$$\begin{aligned} 2K_0 + K_+ &> 4 - \frac{1}{K_-} \\ 2K_0 + K_+ &> 1 \end{aligned} \quad (98)$$

Thus,

$$K_0 > \frac{C_{A_0} - K_+}{2} \quad (99)$$

where  $C_{A_0} = \max\{1, 4 - \frac{1}{K_-}\}$ .

**$A_1$  fixed point**

For  $A_1$  fixed point,

$$\mathcal{O}_{A_1} = \frac{1}{2K_0 + K_+ + K_-} \begin{pmatrix} 2K_0 - K_+ - K_- & -2\sqrt{2K_0K_+} & 2\sqrt{2K_0K_-} \\ -2\sqrt{2K_0K_+} & -2K_0 + K_+ - K_- & -2\sqrt{K_+K_-} \\ 2\sqrt{2K_0K_-} & -2\sqrt{K_+K_-} & 2K_0 + K_+ - K_- \end{pmatrix}. \quad (100)$$

We find that

$$\phi_0 = \sqrt{2}\phi_-, \phi_+ = -\phi_-, \theta_- + \sqrt{2}\theta_0 = \theta_+, \quad (101)$$

and

$$\begin{aligned} \Delta(T_+^s) &= \frac{1 + K_-(2K_0 + K_+)}{2K_0 + K_+ + K_-} \\ \Delta(T_-^s) &= \frac{1 + K_-(2K_0 + K_+)}{2K_0 + K_+ + K_-} \\ \Delta(T_{01}^p) &= 4\left(\frac{1}{K_-} + \frac{1}{2K_0 + K_+}\right)^{-1} \\ \Delta(T_{12}^p) &= 4\left(\frac{1}{K_-} + \frac{1}{2K_0 + K_+}\right)^{-1} \\ \Delta(T_{20}^p) &= 0 \\ \Delta(B_0) &= \frac{4}{2K_0 + K_+ + K_-} \\ \Delta(B_1) &= 0 \\ \Delta(B_2) &= \frac{4}{2K_0 + K_+ + K_-}. \end{aligned} \quad (102)$$

Thus,  $A_1$  fixed point is stable when

$$\begin{aligned} [1 - (2K_0 + K_+)](1 - K_-) &> 0 \\ \frac{1}{K_-} + \frac{1}{2K_0 + K_+} &< 4 \\ 2K_0 + K_+ + K_- &< 4 \end{aligned} \quad (103)$$

Thus,

$$\begin{aligned} \frac{(4 - \frac{1}{K_-})^{-1} - K_+}{2} &< K_0 < \frac{1 - K_+}{2} \\ K_- &> \frac{1}{4} \end{aligned} \quad (104)$$

 **$A_2$  fixed point**

For  $A_2$  fixed point,

$$\mathcal{O}_{A_2} = \frac{1}{2K_0 + K_+ + K_-} \begin{pmatrix} 2K_0 - K_+ - K_- & -2\sqrt{2K_0K_+} & -2\sqrt{2K_0K_-} \\ -2\sqrt{2K_0K_+} & -2K_0 + K_+ - K_- & 2\sqrt{K_+K_-} \\ -2\sqrt{2K_0K_-} & 2\sqrt{K_+K_-} & 2K_0 + K_+ - K_- \end{pmatrix}. \quad (105)$$

and

$$\phi_0 = -\sqrt{2}\phi_-, \phi_+ = \phi_-, \theta_- + \theta_+ = \sqrt{2}\theta_0. \quad (106)$$

Then

$$\begin{aligned}
\Delta(T_+^s) &= 0 \\
\Delta(T_-^s) &= 0 \\
\Delta(T_{01}^p) &= 0 \\
\Delta(T_{12}^p) &= 4\left(\frac{1}{K_-} + \frac{1}{2K_0 + K_+}\right)^{-1} \\
\Delta(T_{20}^p) &= 4\left(\frac{1}{K_-} + \frac{1}{2K_0 + K_+}\right)^{-1} \\
\Delta(B_0) &= \frac{4}{2K_0 + K_+ + K_-} \\
\Delta(B_1) &= \frac{4}{2K_0 + K_+ + K_-} \\
\Delta(B_2) &= 0.
\end{aligned} \tag{107}$$

Thus,  $A_1$  fixed point is stable when

$$\begin{aligned}
\frac{1}{K_-} + \frac{1}{2K_0 + K_+} &< 4 \\
2K_0 + K_+ + K_- &< 4
\end{aligned} \tag{108}$$

It is easy to see that  $A_1$  and  $A_2$  fixed points coexist in the same parameter region.

#### Majorana-free phase diagram without bulk pair-hopping interaction

Now we are ready to map out the phase diagram of DSM nanowire junction without pair-hopping interaction (Majorana-free). As shown in Fig. 3, the phase diagrams are plotted for a fixed  $K_-$  value in: (a)  $K_- = 0.4$ , (b)  $K_- = 0.6$ , (c)  $K_- = 0.8$ , (d)  $K_- = 1$ . Remarkably, the junction is at stable asymmetric  $A_0$  fixed point in the “free fermion” limit with  $K_0 = K_+ = 1$  (red dot), where wire  $i = 0$  is completely disconnected from wire  $i = 1, 2$ . In this weakly interacting region with  $K_- < 1$ , the two-terminal conductance across the junction should be zero.

#### APPENDIX G. PHASE DIAGRAM OF BINDED Y-JUNCTION WITH RMZM

When bulk pair-hopping interaction is incorporated between wire  $i = 1$  and wire  $i = 2$ , the system becomes the binded Y-junction structure. Pair-hopping interaction  $g$  pins  $\theta_-$  to a classical value  $\sqrt{\pi}n_{\theta_-}$ , with  $n_{\theta_-} \in \mathbb{Z}$ . Interestingly, it is possible that certain boundary condition pins  $\phi_-$  to  $\sqrt{\pi}n_{\phi_-}x$  ( $n_{\phi_-} \in \mathbb{Z}$ ) simultaneously at  $x = 0$ , even though  $\theta_-$  and  $\phi_-$  do NOT commute with each other. Such competition between bulk interaction and boundary condition requires promoting both  $n_{\phi_-}$  and  $n_{\theta_-}$  to integer-valued operators to recover the non-commutativity between  $\phi_-$  and  $\theta_-$  at  $x = 0$ . With this subtlety, we briefly summarize our strategy to study the critical behaviors of binded Y-junction:

(1) For a generic tunneling/backscattering operator  $t = \cos \sqrt{\pi}[(m_0\phi_0 + m_+\phi_+ + m_-\phi_-) + (n_0\theta_0 + n_+\theta_+ + n_-\theta_-)]$ . The pinning of  $\theta_-$  is equivalent to setting  $n_- = 0$  in  $t$  in RG calculation.

(2) With  $n_- = 0$ , we force  $\Delta(t)$  (the scaling dimension of  $t$ ) to be zero to arrive at a possible fixed point  $F_t$ , which is characterized by an  $\mathcal{O}_t$  matrix.  $F_t$  is a physical fixed point with  $\Delta(t) = 0$ , only if orthogonality condition  $\mathcal{O}_t^T \mathcal{O}_t = 1$  is satisfied. Otherwise,  $F_t$  is not physical and does not show up in the phase diagram.

(3) Write down the explicit boundary conditions of a physical fixed point, and check that whether the boundary condition forces the pinning of  $\phi_-$ . If pinning of  $\phi_-$  is not required by the boundary condition, any operator  $t$  with  $m_- \neq 0$  is forced to vanish due to strong  $\phi_-$  fluctuations and does not enter the phase diagram.

(4) Use  $\mathcal{O}_t$  to calculate the remaining perturbation terms, and obtain the stability condition of  $F_t$ .

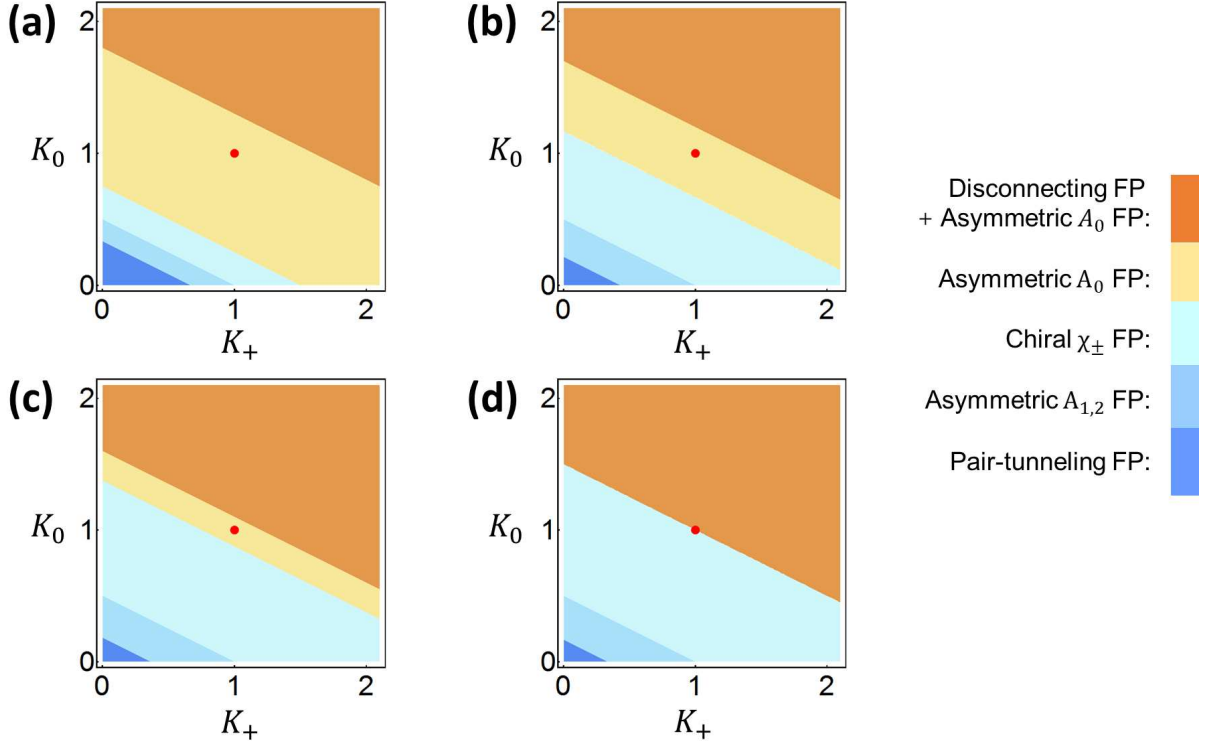


FIG. 3. Majorana-free phase diagram with  $K_-$  value: (a)  $K_- = 0.4$ , (b)  $K_- = 0.6$ , (c)  $K_- = 0.8$ , (d)  $K_- = 1$

#### Why $\chi_+$ fixed point is not physical in binded Y-junction?

To start with, we apply the above criterion to  $\chi_+$  fixed point, and explicitly show that in the presence of pair hopping interaction  $g$ , the rotation matrix of  $\chi_+$  fixed point  $\mathcal{O}_+$  is modified to a non-orthogonal form  $\mathcal{O}_+^{(g)}$ . Recall that  $\chi_+$  fixed point forces trivial scaling dimensions of  $T_+^{0,1,2}$ . Let us first write down

$$\begin{aligned} T_0^+ &\sim \cos \sqrt{\pi} \left[ \frac{\tilde{\chi}_{0,L} + \tilde{\chi}_{0,R}}{2\sqrt{K_0}} + \frac{\sqrt{K_0}}{2} (\tilde{\chi}_{0,L} - \tilde{\chi}_{0,R}) + \frac{\tilde{\chi}_{+,L} + \tilde{\chi}_{+,R}}{2\sqrt{2K_+}} - \frac{\sqrt{K_+}}{2\sqrt{2}} (\tilde{\chi}_{+,L} - \tilde{\chi}_{+,R}) + \frac{\tilde{\chi}_{-,L} + \tilde{\chi}_{-,R}}{2\sqrt{2K_-}} \right] \\ T_1^+ &\sim \cos \sqrt{\pi} \left[ \frac{\tilde{\chi}_{+,L} + \tilde{\chi}_{+,R}}{\sqrt{2K_+}} \right] \\ T_2^+ &\sim \cos \sqrt{\pi} \left[ \frac{\tilde{\chi}_{0,L} + \tilde{\chi}_{0,R}}{2\sqrt{K_0}} - \frac{\sqrt{K_0}}{2} (\tilde{\chi}_{0,L} - \tilde{\chi}_{0,R}) + \frac{\tilde{\chi}_{+,L} + \tilde{\chi}_{+,R}}{2\sqrt{2K_+}} + \frac{\sqrt{K_+}}{2\sqrt{2}} (\tilde{\chi}_{+,L} - \tilde{\chi}_{+,R}) - \frac{\tilde{\chi}_{-,L} + \tilde{\chi}_{-,R}}{2\sqrt{2K_-}} \right] \end{aligned} \quad (109)$$

Notice that  $T_1^+$  takes this form because we have ignored the constant part originated from the pinning of  $\theta_-$ . Together with the current conservation condition, the existence of  $\chi_+$  fixed point requires the following equations to be satisfied

$$\begin{aligned} \frac{\tilde{\chi}_{0,R} + \tilde{\chi}_{0,L}}{2\sqrt{K_0}} + \frac{\tilde{\chi}_{+,R} + \tilde{\chi}_{+,L}}{\sqrt{2K_+}} &= 0 \\ \frac{\tilde{\chi}_{+,L} + \tilde{\chi}_{+,R}}{\sqrt{2K_+}} &= 0 \\ \frac{\tilde{\chi}_{0,L} + \tilde{\chi}_{0,R}}{2\sqrt{K_0}} + \frac{\sqrt{K_0}}{2} (\tilde{\chi}_{0,L} - \tilde{\chi}_{0,R}) + \frac{\tilde{\chi}_{+,L} + \tilde{\chi}_{+,R}}{2\sqrt{2K_+}} - \frac{\sqrt{K_+}}{2\sqrt{2}} (\tilde{\chi}_{+,L} - \tilde{\chi}_{+,R}) + \frac{\tilde{\chi}_{-,L} + \tilde{\chi}_{-,R}}{2\sqrt{2K_-}} &= 0 \end{aligned} \quad (110)$$

This immediately leads to the following solution

$$\begin{aligned} \tilde{\chi}_{0,R} &= -\tilde{\chi}_{0,L}, \quad \tilde{\chi}_{+,R} = -\tilde{\chi}_{+,L} \\ \tilde{\chi}_{-,R} &= -2\sqrt{2K_0K_-}\tilde{\chi}_{0,L} + 2\sqrt{K_+K_-}\tilde{\chi}_{+,L} - \tilde{\chi}_{-,L} \end{aligned} \quad (111)$$

Therefore, the rotation matrix is given by

$$\mathcal{O}_+^{(g)} = \begin{pmatrix} -1 & 0 & 0 \\ 0 & -1 & 0 \\ -2\sqrt{2K_0K_-} & 2\sqrt{K_+K_-} & -1 \end{pmatrix}. \quad (112)$$

It is easy to verify that  $\mathcal{O}_+^{(g)}$  fails to satisfy the orthogonal condition. As a result,  $\chi_+$  fixed point is not physical in the presence of  $g$ , and should not be considered as a candidate of fixed point in the phase diagram. Similar argument can be performed to other fixed points, and we find that  $\chi_{\pm}$  and  $A_{1,2}$  fixed points are unphysical. The analysis of remaining physical fixed points are given below.

### Disconnecting fixed point

With  $n_- = 0$ , we find that the disconnecting fixed point is characterized by the same  $\mathcal{O}_D$  matrix,

$$\mathcal{O}_D = \begin{pmatrix} -1 & 0 & 0 \\ 0 & -1 & 0 \\ 0 & 0 & -1 \end{pmatrix}. \quad (113)$$

The explicit boundary condition is

$$\phi_0 = \phi_+ = \phi_- = 0, \quad (114)$$

where both  $\phi_-$  and  $\theta_-$  are pinned at  $x = 0$ . Therefore,

$$\begin{aligned} \Delta(T_+^s) &= \frac{1}{4}(2K_0 + K_+) \\ \Delta(T_-^s) &= \frac{1}{4}(2K_0 + K_+) \\ \Delta(T_{01}^p) &= 2K_0 + K_+ \\ \Delta(T_{12}^p) &= 0 \\ \Delta(T_{20}^p) &= 2K_0 + K_+ \\ \Delta(B_0) &= 0 \\ \Delta(B_1) &= 0 \\ \Delta(B_2) &= 0. \end{aligned} \quad (115)$$

Notice that the scaling dimensions have been modified compared with Eq. 80. Here  $\Delta(T_{12}^p) = 0$  is a manifestation of pinning  $\theta_-$ , which will also appear in other fixed points. Now, disconnecting fixed point is stable when

$$K_0 > \frac{4 - K_+}{2} \quad (116)$$

### Pair-tunneling fixed point

With  $n_- = 0$ , the  $\mathcal{O}_D$  matrix remain unchanged compared with the  $n_- \neq 0$  case. Thus, we still have

$$\phi_0 = -\sqrt{2}\phi_+, \quad \theta_+ = \sqrt{2}\theta_0, \quad \theta_- = 0, \quad (117)$$

where  $\phi_-$  is not pinned by the boundary condition, and thus will be strongly fluctuating due to the pinning of  $\theta_-$ . Therefore, terms that involve  $\phi_-$ , such as  $T_{\pm}^s$  and  $B_{1,2}$ , will vanish under RG. The only allowed perturbation term at this fixed point is the backscattering term  $B_0$ , with

$$\Delta(B_0) = \frac{4}{2K_0 + K_+} \quad (118)$$

So, pair-tunneling fixed point is stable when

$$K_0 < \frac{4 - K_+}{2} \quad (119)$$

Comparing this stability condition with Eq. 116, we find that disconnecting fixed point and pair-tunneling fixed point are dual to each other.

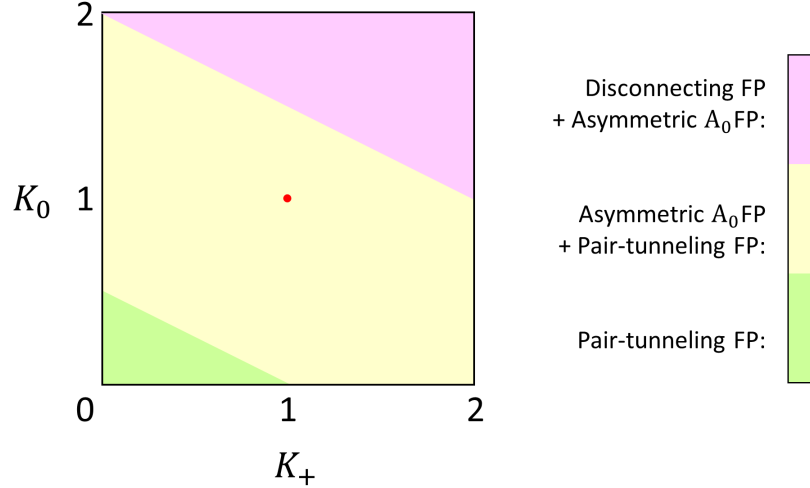


FIG. 4. The phase diagram with rMZM (pair hopping interaction).

#### $A_0$ fixed point

For asymmetric fixed point  $A_0$ ,  $\mathcal{O}_{A_0}$  remains the same with or without the pinning condition  $n_- = 0$ . The explicit boundary condition is

$$\phi_0 = \phi_+ = \theta_- = 0. \quad (120)$$

Then  $\phi_-$  is also strongly fluctuating, and the non-vanishing tunneling processes are pair-tunneling  $T_{01}^p$  and  $T_{20}^p$ , with

$$\Delta(T_{01}^p) = \Delta(T_{20}^p) = 2K_0 + K_+ \quad (121)$$

Thus,  $A_0$  fixed point is stable when

$$2K_0 + K_+ > 1 \quad (122)$$

#### Phase diagram with rMZM

The phase diagram can be easily mapped out in Fig. 4, and quite remarkably, the phase boundaries are completely independent of the value of  $K_-$ , in comparison with Fig. 3. As shown in Fig. 4, in the weak interacting region, the DSM nanowire junction is in the coexisting phase between  $A_0$  fixed point and pair-tunneling fixed point. This signals the emergence of an unstable fixed point which characterizes the phase transition between  $A_0$  fixed point and pair-tunneling fixed point, which is similar to a pinch-off transition.